

# First-Principles Modeling of the Temperature Dependence for the Superlattice Intrinsic Stacking Fault Energies in $L1_2$ $Ni_{75-x}X_xAl_{25}$ Alloys



J.D.T. ALLEN, A. MOTTURA, and A. BREIDI

Stronger and more resistant alloys are required in order to increase the performance and efficiency of jet engines and gas turbines. This will eventually require planar faults engineering, or a complete understanding of the effects of composition and temperature on the various planar faults that arise as a result of shearing of the  $\gamma'$  precipitates. In the current study, a combined scheme consisting of the density functional theory, the quasi-harmonic Debye model, and the axial Ising model, in conjunction with a quasistatic approach is used to assess the effects of composition and temperature of a series of pseudo-binary alloys based on the  $(Ni_{75-x}X_x)Al_{25}$  system using distinct relaxation schemes to assess observed differences. Our calculations reveal that the (111) superlattice intrinsic stacking fault energies in these systems decline modestly with temperature between 0 K and 1000 K.

<https://doi.org/10.1007/s11661-018-4763-4>

© The Minerals, Metals & Materials Society and ASM International 2018

## I. INTRODUCTION

IN precipitation-strengthened alloys, the shearing of particles is often one of the active deformation mechanisms. Superalloys are no exception to this, and their complex shearing mechanisms are indeed partly responsible for their superior mechanical properties at high temperatures. Over the last few decades, increasing focus has been spent on understanding these shearing mechanisms, which change with composition and temperature. The crystal structure of the matrix ( $\gamma$ , fcc) and precipitate ( $\gamma'$ ,  $L1_2$ ) phase is such that a full dislocation in the matrix results in the introduction of an anti-phase boundary (APB) in the precipitate phase. Other partial dislocations can also shear these precipitates, leading to a diverse range of faults: superlattice intrinsic stacking faults (SISFs), superlattice extrinsic stacking faults (SESFs), complex stacking faults (CSFs), which can themselves be intrinsic or extrinsic, twin structures and more complicated planar defects.

The energies of these planar faults are extremely important as they determine the nature of the complex dislocation structures shearing the precipitates, as well as the segregation of solute elements to the fault

energies, which in turns can affect the motion of dislocations through the precipitates. As a result, a number of mechanical properties, such as minimum grain size due to milling, strain hardening and yield stress depend on planar fault energies. Creep resistance is also affected by the planar fault energies.<sup>[1]</sup> As microstructure and processing methods are refined further, it may be possible to achieve even higher strengths and high-temperature properties through planar faults engineering. Therefore, a complete understanding of the effects of composition and temperature on planar fault energies must be developed in order to exploit these opportunities.

Planar fault energies can be measured experimentally, by determining the separation between partials using transmission electron microscopes. However, the thin-film effects and uncertainty about how to apply relevant corrections make this type of experimental study very difficult.<sup>[2-4]</sup> These issues also make it very difficult to systematically study the effect of composition and temperature on these planar fault energies.

On the other hand, recent experimental study has shown robust evidence of solute segregation to these planar faults in the superalloys, often referred to as Suzuki segregation.<sup>[5]</sup> Several studies have successfully employed scanning transmission electron microscopy, often coupled with energy-dispersive spectroscopy, to map solute concentration at SISFs, SESFs, and twin structures in both Ni- and Co-based superalloys.<sup>[6,7]</sup> At the same time, the density functional theory (DFT) has been employed to compute relevant planar fault energies, and to assess the effect of composition on these values. Two main approaches exist for calculating

J.D.T. ALLEN and A. MOTTURA are with the School of Metallurgy and Materials, University of Birmingham, Edgbaston B15 2TT, UK. A. BREIDI is with the UK Atomic Energy Authority, Culham Science Centre, Oxfordshire OX14 3DB, UK. Contact e-mail: a.breidi@hotmail.com

Manuscript submitted March 18, 2018.

planar fault energies using the DFT. A more traditional approach involves calculating the energy differences between a perfect and a faulted supercell, thereby simulating the planar fault explicitly.<sup>[8,9]</sup> An alternative approach is to employ the Ising model to describe the energy of a large supercell as a sum of contributions arising from the interactions of pairs of planes.<sup>[10]</sup> Both methods have been used to compute various planar fault energies and the effect of composition on planar fault energies for  $\gamma'$ -Ni<sub>3</sub>Al-based alloys.<sup>[8,9,11]</sup>

One of the main limitations of the available theoretical studies is that all values are computed at 0 K. This may be a problem since the superalloys are usually operating at appreciable temperatures. Thus, it becomes necessary to assess how these energies may change as temperature is increased. In our recent major study,<sup>[11]</sup> we have established the effect of composition on the SISF energies in all  $\gamma'$ -Ni<sub>3</sub>Al-based alloys at 0 K. We have as well addressed the temperature effect on the SISF energies for several Ni<sub>3</sub>Al-based systems, specifically: (Ni<sub>75-x</sub>Co<sub>x</sub>)Al<sub>25</sub>, (Ni<sub>75-x</sub>Cu<sub>x</sub>)Al<sub>25</sub>, (Ni<sub>75-x</sub>Pd<sub>x</sub>)Al<sub>25</sub>, (Ni<sub>75-x</sub>Pt<sub>x</sub>)Al<sub>25</sub>. However, the current temperature-dependence results (Section IV-B-3<sup>[11]</sup>) are preliminary, since they did not involve local atomic relaxations of the D0<sub>19</sub> structure. Thereby, the SISF energies' temperature dependence presented earlier<sup>[11]</sup> was tentative. In the current study, we try to establish the SISF energies variation as a function of temperature. The investigated alloys are those recently<sup>[11]</sup> addressed: (Ni<sub>75-x</sub>X<sub>x</sub>)Al<sub>25</sub> pseudo-binary system, where X = Co, Cu, Pd, or Pt, and x = 4.62975, 9.2595, 13.88925, and 18.51825 at. pct X. We employ a combined scheme consisting of DFT, the quasi-harmonic Debye (QHD) model, and the axial Ising model (AIM), in conjunction with a quasistatic approach. Furthermore, we assess the effect of relaxations on the overall results by applying two distinct schemes: full internal relaxation where atoms within the structure are allowed to relax to their lowest energy position, and internally static whereby the positions of atoms are kept fixed within the structures.

## II. COMPUTATIONAL METHOD

We combine DFT calculations with the AIM and the QHD model in order to determine the temperature dependence of SISF energies in L1<sub>2</sub> Ni<sub>3</sub>Al-based alloys. This paper does not focus on the methodology behind both models, or on their advantages/disadvantages relative to other approaches (Supercell method and phonon calculations). However, we will adequately introduce the main formalisms of both AIM and QHD models that helped us to have direct access into SISF energies and their thermal dependence. For more details, the reader is referred to References 11 and 12 and references therein.

### A. AIM Model

We employ the axial nearest-neighbor Ising model (ANNI) which is the first-order approximation of the AIM model. The (111) SISF formation energy of L1<sub>2</sub> alloys using the ANNI model is given by

$$\gamma_{ANNI}^{L1_2} = \frac{8(E_{D0_{19}} - E_{L1_2})}{V_{L1_2}^{2/3} \cdot \sqrt{3}}, \quad [1]$$

where  $V_{L1_2}$  is the volume of 4-atoms L1<sub>2</sub> unit cell and  $V_{L1_2}^{2/3} \cdot \sqrt{3}$  is the area of 4-atoms in the L1<sub>2</sub> (111) plane over which the stacking fault extends.  $E_{L1_2}$  and  $E_{D0_{19}}$  are the energies per atom of the L1<sub>2</sub> and D0<sub>19</sub> structures.

### B. QHD Model

The QHD model is able to establish the equation of state of a solid, *i.e.*, the volume temperature dependence  $V = f(T)$  where  $V$  is the equilibrium volume at a given temperature  $T$ . This is achieved through minimizing the non-equilibrium Gibbs function as:

$$\left(\frac{\partial G^*}{\partial V}\right)_{T,P} = 0, \quad [2]$$

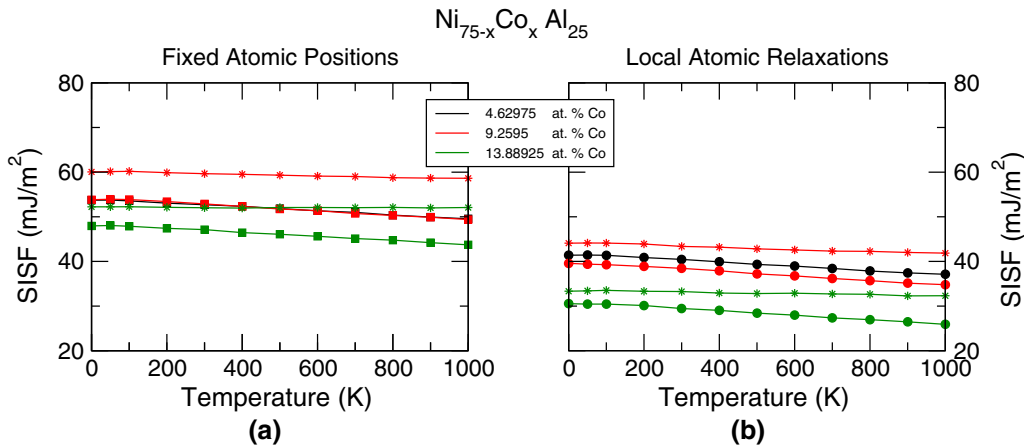


Fig. 1—Variation of the SISF energies as a function of temperature for the System L1<sub>2</sub> Ni<sub>75-x</sub>Co<sub>x</sub>Al<sub>25</sub>. (a) and (b) stand for fixed atomic positions and local atomic relaxations, respectively. The star symbols designate spin-polarized calculations. In (a), the data corresponding to the composition 4.62975 at. pct Co are not visible because they are extremely close to those of 9.2595 at. pct Co. The lines going through the data are purely for visual reasons.

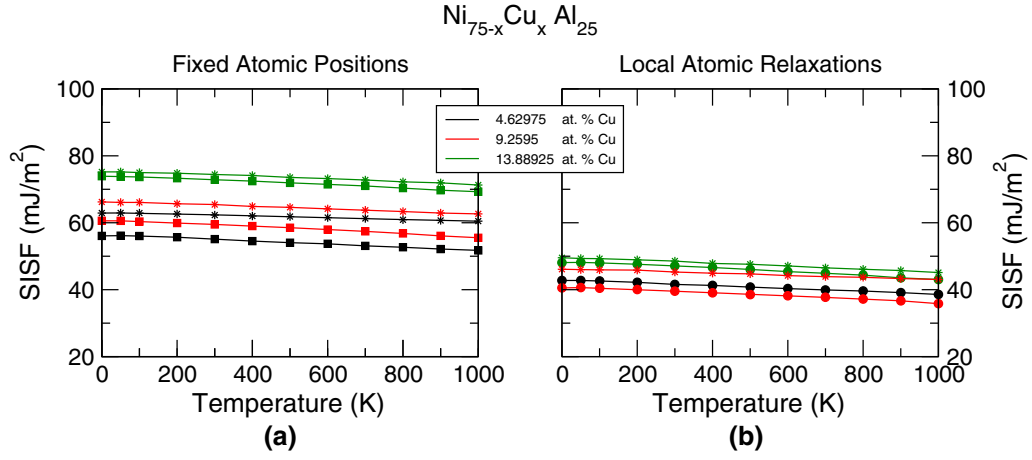


Fig. 2—Change in SISF energies upon temperature increase in the system  $L1_2 \text{Ni}_{75-x}\text{Cu}_x\text{Al}_{25}$ . (a) and (b) stand for fixed atomic positions and local atomic relaxations, respectively. The star symbols designate spin-polarized calculations. The lines going through the data are purely for visual reasons.

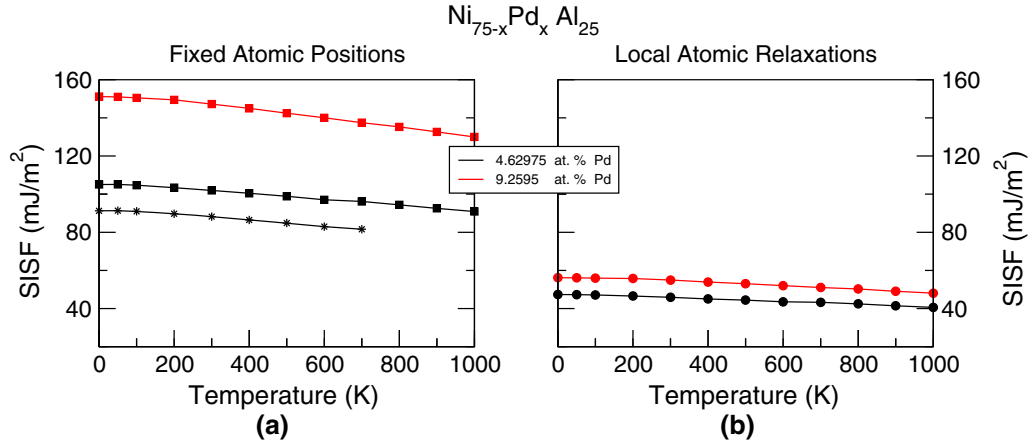


Fig. 3—Temperature dependence of SISF energies in  $L1_2 \text{Ni}_{75-x}\text{Pd}_x\text{Al}_{25}$ . (a) and (b) stand for fixed atomic positions and local atomic relaxations, respectively. The star symbols indicate spin-polarized calculations. The lines connecting the points are only to help guiding the eyes through the data.

where

$$G^*(T, P, V) = E_e(V) + PV + A_{vib}(T, V). \quad [3]$$

$E_e$  is the total energy of the system at a given volume  $V$ , calculated using the DFT.  $P$  is the ambient pressure,  $A_{vib}(T, V)$  is the Helmholtz vibrational energy term. This term is the core-element of the model as it consists of an approximation of the vibrational density of states (DOS) known as Debye's phonon DOS. The minimization of  $G^*$  is implemented in the **gibbs** code.<sup>[13]</sup>

Let's mention here that the computational method presented here was used recently<sup>[11]</sup> to calculate a preliminary temperature dependence of SISF energies in  $L1_2 \text{Ni}_3\text{Al}$ -based alloys, with the exception that in this study we take into account the local atomic relaxations of the  $D0_{19}$  phase, which makes the approach more robust and complete in establishing qualitatively and quantitatively the desired thermal dependence.

### C. Supercell Modeling and First-Principles Techniques

The  $\text{Ni}_{75-x}\text{X}_x\text{Al}_{25}$  alloy was modeled using 108-atom  $L1_2$ -based  $3 \times 3 \times 3 (\times 4\text{-atoms})$  and 216-atom  $D0_{19}$ -based  $3 \times 3 \times 3 (\times 8\text{-atoms})$  supercells. The transition metal ternary element X (Co,Cu,Pd,Pt) occupy exclusively the Ni-sites as the latter manifest strong site-preference to the Ni-sublattice.<sup>[14–17]</sup> In the current study, the alloy compositions fall within the experimental solubility of X in  $\text{Ni}_3\text{Al}$  alloys.<sup>[14]</sup> The used supercells were generated to satisfy the chemical disorder on the Ni-sublattice where the Warren–Cowley short-range order (SRO) parameters<sup>[18,19]</sup> were minimized at several nearest neighbor coordination shells.

The first-principles calculations were performed using the Density-functional theory DFT<sup>[20,21]</sup> as implemented in the Vienna Ab initio Simulation Package (VASP),<sup>[22–24]</sup> which employs the Projector Augmented Wave PAW method to determine the total energies and

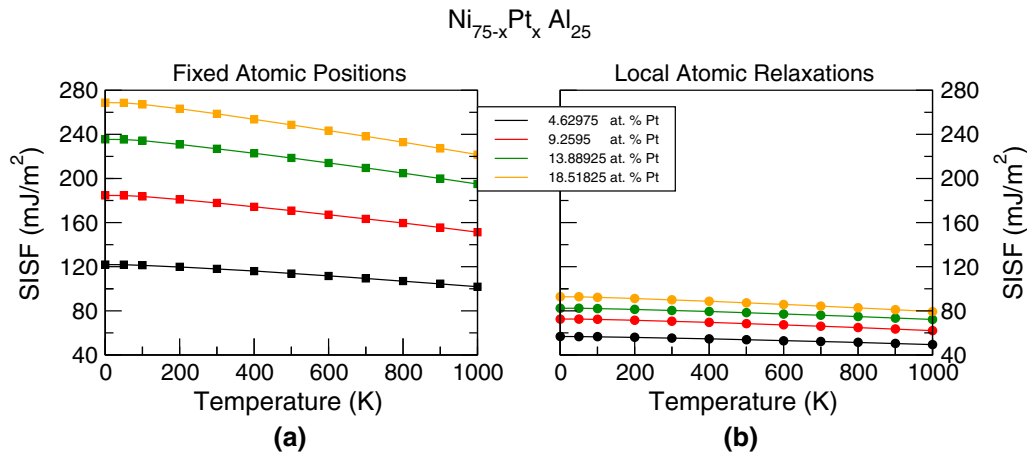


Fig. 4—Temperature dependence of SISF energies in  $L1_2$   $Ni_{75-x}Pt_xAl_{25}$ . (a) and (b) stand for fixed atomic positions and local atomic relaxations, respectively. The lines connecting the points are only to help guide the eyes through the data.

forces. The exchange–correlation (XC) energy of electrons is described in the generalized gradient approximation (GGA) using the functional parameterization of Perdew–Burke–Ernzerhof.<sup>[25]</sup> The energy cut-off was set to 400 eV. A mesh of a 112 and 63 special  $k$ -points for 108-Atom  $L1_2$  and 216-Atom  $D0_{19}$  phases, respectively, were taken in the irreducible wedge of the Brillouin zone for the total energy calculations. These input parameters stabilized the energy differences between  $L1_2$  and  $D0_{19}$  phases and guaranteed the uncertainty in SISF energy to be less than 2 mJ/m<sup>2</sup>.

During relaxation of the  $L1_2$  phase, the supercell shape was kept fixed. Only volume and atomic positions were allowed to change in order to fully minimize the total energy. This technique prevents the  $L1_2$  supercell from deviating to a low symmetric phase.

Concerning the  $D0_{19}$  phase, only local atomic relaxations were allowed. The  $D0_{19}$  volume per atom was intentionally set to the corresponding  $L1_2$  equilibrium value, while the  $c/a$  ratio was kept constant at the  $D0_{19}$  ideal value. This insured that  $a_{D0_{19}}$  and  $c_{D0_{19}}$  correspond to the underlying  $L1_2$  lattice, *i.e.*,  $a_{D0_{19}}/a_{L1_2} = \sqrt{2}$  and  $c_{D0_{19}}/a_{L1_2} = \sqrt{4/3}$ . For both phases, the local atomic relaxations were carried out using the conjugate gradient algorithm,<sup>[26]</sup> a powerful scheme commonly used to relax the atoms into their instantaneous ground states.

### III. RESULTS

The (111) SISF energy temperature dependence in  $L1_2$   $Ni_3Al$ -based alloys is calculated through a combined DFT–AIM–QHD approach. Let us mention here that this approach is quasistatic since the temperature dependence of the SISF energy is obtained through a DFT calculation of the of  $L1_2$  and  $D0_{19}$  energies at a volume  $V$  corresponding to a sought-after temperature  $T$ . Hence, it becomes clear now that this approach assumes that the temperature dependence of SISF energies is attributed only to thermal expansion, *i.e.*,

other thermal effects, namely, electronic, vibrational, and magnetic thermal excitations are not accounted for.

The SISF energy temperature dependence is realized by first feeding the **gibbs** code<sup>[13]</sup> a set of  $L1_2$  Energy–Volume values being determined with VASP code as demonstrated above. **gibbs** will search for an equilibrium volume that minimizes the non-equilibrium Gibbs energy at a given temperature, and hence, volume temperature dependence of lattice  $L1_2$  is established. Then, upon selecting a desired temperature  $T$ , we simulate the  $D0_{19}$  energy with VASP at the corresponding equilibrium volume. Finally, the SISF energy corresponding to a temperature  $T$  is evaluated using the AIM model as expressed by Eq. [1]

Several experimental reports<sup>[27–29]</sup> back this quasistatic approach. It has been shown to be effective in calculating the elastic constants of  $Ni_3Al$ .<sup>[30,31]</sup> It has been as well shown to be successful when calculating the elastic constants of Ta<sup>[32]</sup> where thermal expansivity was the dominant temperature contribution, while other thermal effects such as phonon and electronic excitation contributions were found to be quite minor at constant volume. Of particular importance to this study is the recent success in applying this approach to calculate the SISF energies in unaries,<sup>[33]</sup> pure compounds,<sup>[12]</sup> and alloys<sup>[34]</sup> characterized by complex magnetic structures.

Figures 1 through 4 present the SISF energy temperature dependence of the  $L1_2$   $Ni_{75-x}Co_xAl_{25}$ ,  $Ni_{75-x}Cu_xAl_{25}$ ,  $Ni_{75-x}Pd_xAl_{25}$  and  $Ni_{75-x}Pt_xAl_{25}$  alloys, respectively. Some of the compositions studied, taking into account the volume relaxation only, (*i.e.*, with atomic positions fixed, as in the left panels of Figures 1 through 4), have been preliminarily reported by us.<sup>[11]</sup> The first thing to notice upon analyzing the results is the significant reduction in SISF energies upon performing local atomic relaxations observed in all compositions and systems. It is worth mentioning at this point that the values predicted with local-atomic-relaxation scheme should be more close to the experimental values. The magnitude of the reduction varies significantly between the studied systems and across the alloying compositions. The reduction is highly pronounced in

$\text{Ni}_{75-x}\text{Pd}_x\text{Al}_{25}$  and  $\text{Ni}_{75-x}\text{Pt}_x\text{Al}_{25}$ , and less pronounced in  $\text{Ni}_{75-x}\text{Co}_x\text{Al}_{25}$  and  $\text{Ni}_{75-x}\text{Cu}_x\text{Al}_{25}$ . For the sake of comparison, consider the composition 13.88925 at. pct. Given this composition, the average difference (across temperature) between volume and local-atomic-relaxation schemes reaches a value of as large as 138 mJ/m<sup>2</sup> when substituting Ni by Pt, in comparison with 26 mJ/m<sup>2</sup> when substituting Ni by Cu.

The drop in the calculated SISF energies due to inclusion of atomic relaxations can be explained in terms of the size-argument, *i.e.*, the atomic-radius mismatch. If we consider the system  $\text{Ni}_{75-x}\text{Pt}_x\text{Al}_{25}$ , Pt atoms characterized by large Wigner–Seitz (WS) radii (1.5319 Å) are substituting small Ni atoms (WS = 1.3756 Å), and this atomic-size mismatch is responsible for important atomic relaxations leading the system into its lowest energy configuration which is very much different from that of fixed atomic positions calculations. While, Cu is characterized by WS = 1.4107 Å which is not much larger than Ni (WS = 1.3756 Å), hence, the effect of local-atomic-relaxations is less pronounced in comparison with systems having Pt and Pd (1.52 Å) as alloying elements. We need to emphasize here that we have derived the equilibrium Wigner–Seitz radii (WS) from the room-temperature (RT) experimental atomic volumes<sup>[35]</sup> ( $V_{exp}^{RT} = \frac{4}{3}\pi WS^3$ ) of the alloying element’s ground-state structure.

On the other hand, the variation of the local-atomic-relaxation SISF energies upon increasing temperature exhibits a small linear decrease relative to 0 K values for the whole studied compositions. The magnitude of this decrease barely reaches 10 mJ/m<sup>2</sup> at its maximum. In fact, in our previous investigation,<sup>[11]</sup> we have shown that the change in SISF energies as a function of alloying compositions, upon allowing local-atomic-relaxations, for the solutes Co, Cu, Pd, and Pt is not significant, which is in contrast to the large increase induced by solutes substituting for Al sites. Consequently, it follows from the results presented here and Reference 11 that both alloying and temperature effects have little impact on changing the SISF energies in  $\text{Ni}_{75-x}\text{X}_x\text{Al}_{25}$  alloys.

#### IV. CONCLUSIONS

A combined computational scheme consisting of DFT, QHD, and AIM in conjunction with a quasistatic approach enabled us to establish the temperature dependence of SISF energies in  $\text{L1}_2$   $\text{Ni}_{75-x}\text{X}_x\text{Al}_{25}$  alloys. We find that a proper relaxation of both  $\text{L1}_2$  and  $\text{D0}_{19}$  phases is indispensable to predict a reliable estimation of the SISF energies. Our results, without an exception, all display a linear decline of the SISF energies as a function of composition. Interestingly, this decline is very modest, on average, being less than 10 mJ/m<sup>2</sup> (SISF value at 1000 K relative to 0 K). This insignificant decrease in SISF energies and consequently the minor effect of temperature on the 0 K value are encouraging, as it reduces drastically the computational cost required to calculate the SISF energies at every single

temperature. Hence, it seems plausible to consider the 0 K SISF energy of a  $\text{L1}_2$  multicomponent alloy  $(\text{Ni,Cu,Pd,Pt})_{75}\text{Al}_{25}$  valid to use in physics-based deformation models<sup>[36]</sup> needed to predict primary creep of Ni-superalloys at their operating temperatures. We assert that this conclusion is only valid for alloying elements substituting for Ni-sites, and therefore cannot be extended to include elements substituting for Al-sites. We also emphasize that the current SISF energy temperature dependence is based on volume expansion as the only thermal effect.

#### ACKNOWLEDGMENTS

This study made use of these computational facilities: (a) the University of Birmingham’s BlueBEAR HPC service (<http://www.birmingham.ac.uk/bear>), (b) MidPlus Regional HPC Center ([www.hpc-midlands-pl.us.ac.uk](http://www.hpc-midlands-pl.us.ac.uk)), and (c) Beskow cluster (<https://www.pdc.kth.se/hpc-services/computing-systems/beskow-1.737436>). The authors are therefore very much grateful and would like to thank them for making this study possible. The authors would like, as well, to thank the EPSRC (Grant EP/M021874/1) and EU FP7 (Grant GA109937) for their financial support. Part of this study (A. Breidi) has been carried out within the framework of the EUROfusion Consortium and has received funding from the Euratom research and training programme 2014-2018 under the Grant Agreement No. 633053 and from the RCUK Energy Programme [Grant Number EP/P012450/1]. The views and opinions expressed herein do not necessarily reflect those of the European Commission.

#### REFERENCES

1. C.M.F. Rae and R.C. Reed: *Acta Mater.*, 2007, vol. 55 (3), pp. 1067–81, <https://doi.org/10.1016/j.actamat.2006.09.026>.
2. L. Vitos, J.O. Nilsson, and B. Johansson: *Acta Mater.*, 2006, vol. 54, pp. 3821–26, <https://doi.org/10.1016/j.actamat.2006.04.013>.
3. Y. Qi and R.K. Mishra: *Phys. Rev. B*, 2007, vol. 75, pp. 224105–10, <https://doi.org/10.1103/PhysRevB.75.224105>.
4. C.B. Carter and S.M. Holmes: *Philos. Mag.*, 1977, vol. 35, pp. 1161–72, <https://doi.org/10.1080/14786437708232942>.
5. H. Suzuki: *J. Phys. Soc. Jpn.*, 1962, vol. 17, pp. 322–25, <https://doi.org/10.1143/JPSJ.17.322>.
6. V.A. Vorontsov, L. Kovarik, M.J. Mills, and C.M.F. Rae: *Acta Mater.*, 2012, vol. 60 (12), pp. 4866–78, <https://doi.org/10.1016/j.actamat.2012.05.014>.
7. G.B. Viswanathan, R. Shi, A. Genc, V.A. Vorontsov, L. Kovarik, C.M.F. Rae, and M.J. Mills: *Scripta Mater.*, 2015, vol. 94, pp. 5–8, <https://doi.org/10.1016/j.scriptamat.2014.06.032>.
8. N.C. Eurich and P.D. Bristowe: *Scripta Mater.*, 2015, vol. 102 (Supplement C), pp. 87–90, <https://doi.org/10.1016/j.scriptamat.2015.02.020>.
9. K. V. Vamsi and S. Karthikeyan: in *Superalloys 2012*. Wiley, 2012, pp. 521–30. <https://doi.org/10.1002/9781118516430.ch57>.
10. P.J.H. Denteneer and W. van Haeringen: *J. Phys. C*, 1987, vol. 20 (32), p. L883.
11. A. Breidi, J. Allen, and A. Mottura: *Acta Mater.*, 2018, vol. 145, pp. 97–108, <https://doi.org/10.1016/j.actamat.2017.11.042>.
12. A. Breidi, J. Allen, and A. Mottura: *Phys. Status Solidi (b)*, 2017, <https://doi.org/10.1002/psb.201600839>.

13. M.A. Blanco, E. Francisco, and V. Luaña: *Comput. Phys. Commun.*, 2004, vol. 158 (1), pp. 57–72, <https://doi.org/10.1016/j.comphy.2003.12.001>.
14. Y. Mishima, S. Ochiai, and T. Suzuki: *Acta Metall.*, 1985, vol. 33 (6), pp. 1161–69, [https://doi.org/10.1016/0001-6160\(85\)90211-1](https://doi.org/10.1016/0001-6160(85)90211-1).
15. A.V. Ruban, V.A. Popov, V.K. Portnoi, and V.I. Bogdanov: *Philos. Mag.*, 2014, vol. 94 (1), pp. 20–34, <https://doi.org/10.1080/14786435.2013.838647>.
16. C. Jiang and B. Gleeson: *Scripta Mater.*, 2006, vol. 55 (5), pp. 433–36, <https://doi.org/10.1016/j.scriptamat.2006.05.016>.
17. A.V. Ruban and H.L. Skriver: *Phys. Rev. B*, 1997, vol. 55, pp. 856–74, <https://doi.org/10.1103/PhysRevB.55.856>.
18. J.M. Cowley: *J. Appl. Phys.*, 1950, vol. 21 (1), pp. 24–30, <https://doi.org/10.1063/1.1699415>.
19. B.E. Warren: *X-ray Diffraction*, Dover, New York, 1990.
20. P. Hohenberg and W. Kohn: *Phys. Rev.*, 1964, vol. 136 (3B), pp. B864–71, <https://doi.org/10.1103/PhysRev.136.B864>.
21. W. Kohn and L.J. Sham: *Phys. Rev.*, 1965, vol. 140 (4A), pp. A1133–38, <https://doi.org/10.1103/PhysRev.140.A1133>.
22. G. Kresse and D. Joubert: *Phys. Rev. B*, 1999, vol. 59, pp. 1758–75, <https://doi.org/10.1103/PhysRevB.59.1758>.
23. G. Kresse and J. Furthmüller: *Comput. Mater. Sci.*, 1996, vol. 6 (1), pp. 15–50, [https://doi.org/10.1016/0927-0256\(96\)00008-0](https://doi.org/10.1016/0927-0256(96)00008-0).
24. P.E. Blöchl: *Phys. Rev. B*, 1994, vol. 50, pp. 17953–79, <https://doi.org/10.1103/PhysRevB.50.17953>.
25. J.P. Perdew, K. Burke, and M. Ernzerhof: *Phys. Rev. Lett.*, 1996, vol. 77 (18), pp. 3865–68, <https://doi.org/10.1103/PhysRevLett.77.3865>.
26. W.H. Press, S.A. Teukolsky, W.T. Vetterling, and B.P. Flannery: *Numerical Recipes 3rd Edition: The Art of Scientific Computing*, Cambridge University Press, Cambridge, 2007. ISBN 9780521880688.
27. C.A. Swenson: *J. Phys. Chem. Solids*, 1968, vol. 29 (8), pp. 1337–48, [https://doi.org/10.1016/0022-3697\(68\)90185-6](https://doi.org/10.1016/0022-3697(68)90185-6).
28. E. F. Wasserman: in *Handbook of Ferromagnetic Materials, Handbook of Ferromagnetic Materials*, vol. 5. Elsevier, 1990, pp. 237–322. [https://doi.org/10.1016/s1574-9304\(05\)80063-x](https://doi.org/10.1016/s1574-9304(05)80063-x).
29. O.L. Anderson and D.G. Isaak: *Elastic Constants of Mantle Minerals at High Temperature*. American Geophysical Union, 2013, pp. 64–97. ISBN 9781118668191. <https://doi.org/10.1029/rf002p0064>.
30. Y. Wang, J. J. Wang, H. Zhang, V. R. Manga, S. L. Shang, L.-Q. Chen, and Z.-K. Liu: *J. Phys.*, 2010, vol. 22(22), art. no. 225404.
31. S.-L. Shang, H. Zhang, Y. Wang, and Z.-K. Liu: *J. Phys.*, 2010, vol. 22(37), art. no. 375403.
32. O. Gülseren and R. E. Cohen.: *Phys. Rev. B*, 2002, vol. 65, art. no. 064103, <https://doi.org/10.1103/physrevb.65.064103>.
33. I. Bleskov, T. Hickel, J. Neugebauer, and A. Ruban.: *Phys. Rev. B*, 2016, vol. 93, art. no. 214115, <https://doi.org/10.1103/physrevb.93.214115>.
34. V. I. Razumovskiy, A. Reyes-Huamantínco, P. Puschnig, and A. V. Ruban.: *Phys. Rev. B*, 2016, vol. 93, art. no. 054111, <https://doi.org/10.1103/physrevb.93.054111>.
35. C. Kittel: *Introduction to Solid State Physics*, 7th ed., Wiley, New York, 1996.
36. Y.-K. Kim, D. Kim, H.-K. Kim, C.-S. Oh, and B.-J. Lee: *Int. J. Plast.*, 2016, vol. 79, pp. 153–75, <https://doi.org/10.1016/j.jiplas.2015.12.008>.